ACS APPLIED MATERIALS & INTERFACES

Research Article

Cite This: ACS Appl. Mater. Interfaces 2018, 10, 11280−11288

www.acsami.org

Superhydrophobic Paper from Nanostructured Fluorinated Cellulose Esters

Pegah Khanjani,[†] Alistair W. T. King,[‡] Gabriel J. Partl,[‡] Leena-Sisko Johansson,[†] Mauri A. Kostiainen,[†,§] and Robin H. A. Ras*[,†,§]

[†]Department of Bioproducts and Biosystems, Aalto University School of Chemical Engineering, Kemistintie 1, 02150 Espoo, Finland

[‡]Department of Chemistry, University of Helsinki, AI Virtasen Aukio 1, 00014 Helsinki, Finland

[§]Department of Applied Physics, Aalto University School of Science, Puumiehenkuja 2, 02150 Espoo, Finland

Supporting Information

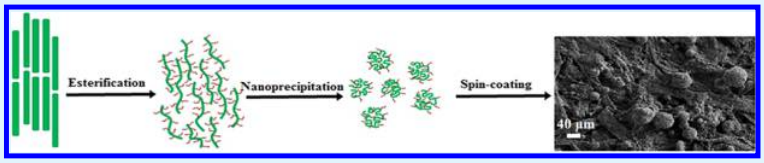

ABSTRACT: The development of economically and ecologically viable strategies for superhydrophobization offers a vast variety of interesting applications in self-cleaning surfaces. Examples include packaging materials, textiles, outdoor clothing, and microfluidic devices. In this work, we produced superhydrophobic paper by spin-coating a dispersion of nanostructured fluorinated cellulose esters. Modification of cellulose nanocrystals was accomplished using 2*H*,2*H*,3*H*,3*H*-perfluorononanoyl chloride and 2*H*,2*H*,3*H*,3*H*-perfluoroundecanoyl chloride, which are well-known for their ability to reduce surface energy. A stable dispersion of nanospherical fluorinated cellulose ester was obtained by using the nanoprecipitation technique. The hydrophobized fluorinated cellulose esters were characterized by both solid- and liquid-state nuclear magnetic resonance, Fourier transform infrared spectroscopy, X-ray photoelectron spectroscopy, and contact angle measurements. Further, we investigated the size, shape, and structure morphology of nanostructured fluorinated cellulose esters by dynamic light scattering, scanning electron microscopy, and X-ray diffraction measurements.

KEYWORDS: *paper, water-repellent, fluorinated cellulose ester, nanoprecipitation, spin-coating*

1. INTRODUCTION

Water droplets roll off easily from superhydrophobic surfaces, which are characterized by high contact angle (>150°) and low contact angle hysteresis.[1−9] The lotus leaf is a primary example of such a superhydrophobic surface found in nature. The surface of the lotus leaf consists of microscale papillae that are coated with hydrophobic wax nanocrystals. The structure of natural superhydrophobic surfaces can be mimicked to create artificial hydrophobic and superhydrophobic materials. Superhydrophobicity of cellulosic materials,[10] based on the generation of roughness, can be classified into two categories.[11] First, cellulosic substrates can be coated with nano-/microstructures using chemical grafting, sol−gel processing, nanoparticle (NP) deposition, and chemical vapor deposition. Second, regeneration and fragmentation of cellulosic materials create roughness, such as in electrospinning or electrospraying of cellulose materials, cellulose nanocrystals (CNCs), and composites.

Many physical and chemical techniques have been developed for the fabrication of hydrophobic/superhydrophobic paper surfaces,[12,13] for example, via plasma treatment,[14] constructing a microstructure surface by microsized $CaCO_3$ and fatty acid,[15] with spraying rapid extension of supercritical CO_2 containing alkyl ketene dimer (AKD),[16,17] chemical vapor deposition of silica particles and polymers,[18] dip-coating with AKD,[19] or surface-coating by grafting polymers.[20,21] Among these techniques, cellulose esterification is a simple and efficient technique for fabricating superhydrophobic paper that requires no special equipment.[22] The hydrophilicity and dispersibility of cellulose can easily be modified by substitution of the hydroxyl groups with different functional groups.[23−25] Research on superhydrophobic paper utilizing biopolymers and sustainable raw materials, such as cellulose, is a fairly new area, and only a limited number of publications are available in the literature.[22] All the mentioned techniques deal with the first category to attain superhydrophobicity.

Recently, Geissler et al. prepared superhydrophobic surfaces from microcrystalline cellulose (MCC) (50 μm) to produce nanostructured cellulose stearoyl esters.[22] Simultaneously, they fabricated thermoresponsive superhydrophobic paper using dip-coating and then spray-coating paper by these nanostructured cellulose stearoyl esters.[22] Because superhydrophobic properties are based on surface nano- and/or microstructures, they utilized nanoprecipitation as an efficient

Received: December 19, 2017
Accepted: March 8, 2018
Published: March 8, 2018

DOI: 10.1021/acsami.7b19310
ACS Appl. Mater. Interfaces 2018, 10, 11280−11288

technique to convert cellulose derivatives into NPs. Nanoprecipitation is based on the addition of a nonsolvent to a dispersion of cellulose to form nanostructured aggregates. They prepared cellulose stearoyl ester NPs from MCC by applying this nanoprecipitation technique with different solvents such as dichloromethane and acetone. Three different techniques, spray-coating, spin-coating, and solvent-casting, were utilized to fabricate superhydrophobic films on glass slides.[26]

Baidya et al. developed multifunctional waterproof paper via functionalization of cellulose nanofibers with fluoroalkyl trialkoxysilane directly in the aqueous suspension,[13] which may reduce environmental concerns but may slightly limit flexibility of the process. However, in current work, we present an initial proof of concept. We have also developed a good understanding of the chemistry involved which, when optimized, could lead to something which is industrially feasible. In addition to the paper-coating, we were also able to make superhydrophobic textiles (Figure S13), as our process is not restricted to in situ surface modification but offers the potential for coating a wider range of substrates through nanoprecipitation.

Moreover, in most of the mentioned methods, complicated manufacturing processes (high temperature or/and pressure, require cleaning room), cost, and surface compatibility may restrict the use of these methods in industrial applications. Thus, nanoprecipitation offers some flexibility if the fluorinated material can be prepared economically and is environmentally benign.

In this study, the hydrophobic and superhydrophobic coating of paper surface was achieved through the heterogeneous synthesis of fluorinated cellulose esters from unmodified CNCs with a larger reactive surface area (5−8 nm in diameter and 50−500 nm in length).[27] Our overall target was to form nanospherical fluorinated cellulose ester prior to coating the obtained materials on the substrate via nanoprecipitation. We successfully demonstrated that the fluorinated cellulose ester could be produced through a heterogeneous reaction, which is promising for further optimization, as heterogeneous processes typically have much more favorable economics than homogeneous processes, for example, those involving LiCl/DMA or ionic liquid.

Spin-coating of the resulting stable colloidal solution on paper substrates led to a uniform superhydrophobic surface. Moreover, we also present that the resulting superhydrophobic fluorinated cellulose esters are stable at high temperature and under strongly acidic and alkaline conditions (Figure S14) for a period of time.

2. EXPERIMENTAL SECTION

2.1. Materials. CNCs were prepared from ground Whatman 541 ashless filter paper using a published method,[28] and the nanocrystals were recovered by freeze-drying from water dispersions. Typical dimensions of the CNCs are in the range of 5−8 nm in diameter and 50−500 nm in length.[27] This leads to high aspect ratios (diameter/length) of around 10−100 and a large reactive surface area. 2*H*,2*H*,3*H*,3*H*-Perfluoroundecanoyl chloride (97%), 2*H*,2*H*,3*H*,3*H*-perfluorononanoic acid (96%), thionyl chloride, toluene, and pyridine were used as received (Sigma-Aldrich). The synthesis and characterization of 2*H*,2*H*,3*H*,3*H*-perfluorononanoyl chloride and cellulose 2*H*,2*H*,3*H*,3*H*-perfluoroundecanoyl ester are presented in the Supporting Information (Figures S1−S5).

2.2. Synthesis of Cellulose 2*H*,2*H*,3*H*,3*H*-Perfluorononanoyl Ester. Freeze-dried CNCs (200 mg) were dispersed in 10 mL of pyridine. Then, the cellulose dispersion was heated to 80 °C. 2*H*,2*H*,3*H*,3*H*-Perfluorononanoyl chloride (1.5 g, 3.65 mmol) (Supporting Information Figure S1) was dissolved in 10 mL of toluene and then added dropwise into the hot cellulose dispersion. Addition was carried out under nitrogen atmosphere. After 24 h, the reaction mixture was allowed to cool down to room temperature (RT) and poured into 100 mL of toluene. The precipitate was purified through repeated dispersion in dichloromethane, precipitation with ethanol and centrifugation cycles. The dried reaction products were characterized by Fourier transform infrared (FTIR) and nuclear magnetic resonance (NMR). The structure of the esterified cellulose is shown in Figure 1.

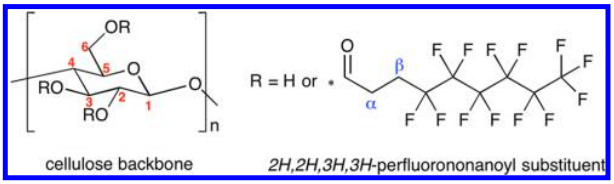

Figure 1. Proposed structure of the 2*H*,2*H*,3*H*,3*H*-perfluorononanoyl cellulose formed under heterogeneous reaction conditions in toluene/pyridine by reaction with acid chloride.

2.3. NP Preparation. Fluorinated CNCs were first dispersed into tetrahydrofuran (THF) at a concentration of 25 mg/mL. The dispersions were filtered through a filter paper with a pore size of 1 μm in a Buchner funnel under vacuum.[29] After filtration, 10 mL of solution was precipitated drop by drop into 250 mL of deionized water at RT. The dispersion was then stirred for 30 min at RT and then heated to 75 °C for 30 min to evaporate most THF and promote nanoprecipitation.

2.4. Superhydrophobic Film Preparation. Superhydrophobic surfaces were prepared by dispersing modified cellulose in THF at a concentration of 25 mg/mL. Cellulose dispersion (50 mL) was then precipitated into 250 mL of ethanol at RT with vigorous stirring for a further 30 min, leading to a white dispersion. Then, spin-coating was carried out on the Staples A4 80 gsm multipurpose paper surface at 4000 rpm for 1 min using a Laurell spin-coater WS-650SX-6NPP-Lite (Laurell Technologies Corp., North Wales, PA). Thereafter, it was dried at 80 °C, and spin-coating was repeated for 10 min.

2.5. NMR Analysis. Solid-state ^{13}C cross-polarizing magic-angle spinning (^{13}C CP MAS) NMR experiments were recorded using a Bruker AVANCE 400 spectrometer. Liquid-state NMR analysis of the prepared acid chloride and cellulose fluoroester was performed using a Varian Inova 600 MHz spectrometer. Standard ^{1}H NMR experiments and diffusion-edited ^{1}H experiments were run using a 5 mm triple resonance probe head. Quantitative ^{13}C NMR experiments were run using a 5 mm broad-band probe head. The liquid-state NMR was achieved after dissolution into an ionic liquid electrolyte containing tetra-*n*-butyl phosphonium acetate ([P_{4444}][OAc]/DMSO-d_6 (1:4 w/w). The synthesis of [P_{4444}][OAc] was performed according to a previous publication.[30] Cellulose assignments using a similar solvent system can be found in our previous work.[31] Full details of the preparation of the reagents, the NMR solutions, and experimental details are given in the Supporting Information. Diffusion-edited ^{1}H experiments refer to a standard convection compensated bipolar pulse pair stimulated echo (CC-BPPSTE)[32,33] diffusion-ordered spectroscopy (DOSY) NMR experiment where the conditions are optimized to allow for complete removal of the fast diffusing species (mainly DMSO and ionic liquid) at the final diffusion gradient. Repeated transients are collected at this final gradient to yield a spectrum containing only the polymeric resonances, aside from a few remaining artifacts.

2.6. Fourier Transform Infrared Spectroscopy. Transmission spectra were recorded on a Nicolet Magna 750 spectrometer using an attenuated total reflection setup. Air background spectra were acquired before each set of measurements.

2.7. X-ray Diffraction. X-ray diffraction (XRD) analysis of the samples was carried out using PANalytical X'Pert Pro MPD Cu K_α radiation. The spectra were collected in a 2θ range of 2°−70°.

DOI: 10.1021/acsami.7b19310
ACS Appl. Mater. Interfaces 2018, 10, 11280−11288

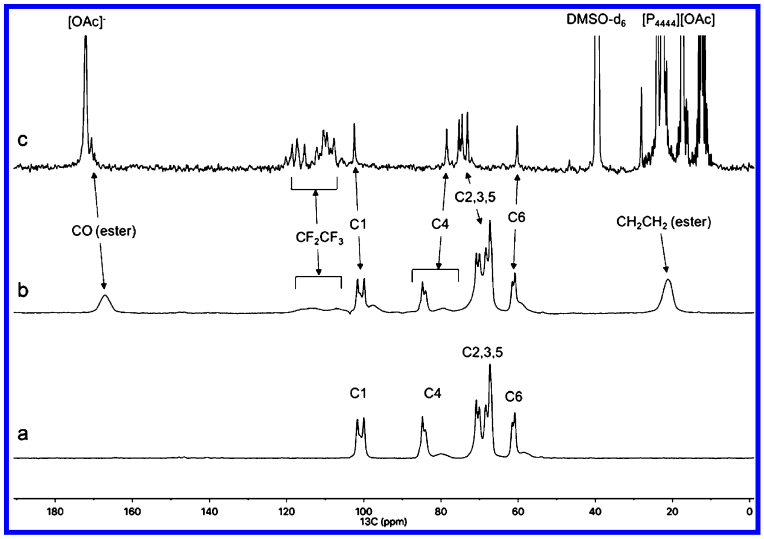

Figure 2. Solid-state ^{13}C NMR spectra of native CNCs (a), cellulose 2*H*,2*H*,3*H*,3*H*-perfluorononanoyl ester (b), and liquid-state ^{13}C NMR spectrum of the cellulose 2*H*,2*H*,3*H*,3*H*-perfluorononanoyl ester dissolved in the electrolyte $[P_{4444}][OAc]$/DMSO-d_6 (1:4 w/w) (c).

2.8. Scanning Electron Microscopy. Experiments were performed with a Zeiss Sigma VP field-emission scanning electron microscope operating at 1 kV.

2.9. Procedure of Sample Preparation for SEM Measurement. The initial concentration of fluorinated cellulose esters in THF was 25 mg/mL. Each dispersion (10 mL) was precipitated drop by drop into 250 mL of deionized water separately, and THF was removed by evaporation. Each sample (600 μL) in deionized water was dropped separately onto the mica substrate. After drying all the samples, they were coated with a thin Au layer for 40 s.

2.10. Dynamic Light Scattering. Nanostructured fluorinated cellulose esters in deionized water were measured on a Nanosizer (Malvern Instrument Ltd., U.K.) after filtering with a pore size of 1 μm. The filtered solution (1 mL) was used for the measurement.

2.11. Contact Angle Measurement. Advancing and receding contact angles were measured using the sessile droplet method (Attension Theta optical tensiometer, Espoo, Finland).[34]

2.12. XPS Measurements. Surface composition of the fluorinated cellulose ester was evaluated using the AXIS Ultra instrument (Kratos Analytical, U.K.). A sample, deposited on paper, was mounted on a sample holder using an ultrahigh vacuum-compatible carbon tape and pre-evacuated overnight. A fresh piece of pure cellulosic filter paper (Whatman) was analyzed as an in situ reference. Measurements were performed using monochromated Al Kα irradiation at 100 W and under neutralization. Wide scans as well as high-resolution regions of C 1s, O 1s, and F 1s were recorded on several locations with a nominal analysis area of 400 × 800 μm^2. Analysis depth of the method is less than 5 nm. Data analysis was performed with CasaXPS, and all binding energies were charge-corrected using the main cellulosic C−O component at 286.7 eV as the reference.

3. RESULTS AND DISCUSSION

We found that the mixture of toluene and pyridine was a suitable reaction medium for esterification of the CNCs with C9 and C11 partially fluorinated long-chain aliphatic acid chlorides. Furthermore, we attempted to convert the fluorinated cellulose esters into nanospheres via a nanoprecipitation technique. The reaction resulting in 2*H*,2*H*,3*H*,3*H*-perfluorononanoyl cellulose ester was chosen for further studies, as it yielded a highly dispersible cellulose ester that allowed for formation of nanospheres through the nanoprecipitation technique. Superhydrophobization with the 2*H*,2*H*,3*H*,3*H*-perfluorononanoyl cellulose ester was carried out subsequently by the spin-coating paper surface with the nanospherical fluorinated cellulose ester.

3.1. Synthesis and Characterization of 2*H*,2*H*,3*H*,3*H*-Perfluorononanoyl Cellulose Esters. Cellulose esterification was carried out in the mixture of toluene and pyridine. The reaction was heterogeneous as a homogeneous solution was not obtained at any point during the reaction, that is, CNCs were modified on the surface but did not reach complete conversion to a soluble cellulose ester. FTIR and NMR spectroscopy confirmed the presence of both modified and unmodified cellulose C2,3,6 positions.

As shown in Figure S1, the FTIR spectrum of fluorinated cellulose esters shows the signal at 1750 cm^{-1}, which is attributed to the carbonyl of the ester group of cellulose 2*H*,2*H*,3*H*,3*H*-perfluorononanoyl esters. The signals at 1233, 1200, 1317, and 1334 cm^{-1} are assigned to the fluorinated alkyl chains. IR ν_{max} (cm^{-1}): 735.40 (m, C−C rocking vibrations), 1142.54 (s, C−O−C), 1150 (s, CF_2), 703.8−1204.5 (CF_3), 1427.54 (CH_2CO), 1750.86 (s, C═O), 3339.85 (m, OH).

Besides the IR analysis, the chemical structure of the fluorinated cellulose esters was also studied using both liquid- and solid-state ^{13}C NMR spectroscopy (Figures 2 and S3). The solid-state spectra (Figure 2b) include resonance peaks in the range of 55−110 ppm, corresponding to the cellulose backbone carbon atoms (C−C6). The region from 105 ppm (just downfield from cellulose C1 at 100 ppm) to 120 ppm closely corresponds to the fluorinated carbon region, which is expected for the CF_2 & CF_3 functionalities on the proposed ester side chains. Finally, the cellulose ester samples reveal additional broad resonances, one near 173 ppm, which is characteristic for the ester group and one in the range of 20−35 ppm, which is characteristic for the α and β carbons in the proposed unfluorinated ester methylene units. It is obvious that both the unmodified and modified CNCs (Figure 2a,b) show pronounced signals at 82 ppm, which are characteristic of the crystalline and amorphous conformers of the cellulose C4.

The resonance at 173 ppm is attributed to C═O. This is more intense in the cellulose 2*H*,2*H*,3*H*,3*H*-perfluorononanoyl ester than the cellulose 2*H*,2*H*,3*H*,3*H*-perfluoroundecanoyl ester, relative to the cellulose backbone signals (Figure S3).

DOI: 10.1021/acsami.7b19310
ACS Appl. Mater. Interfaces 2018, 10, 11280−11288

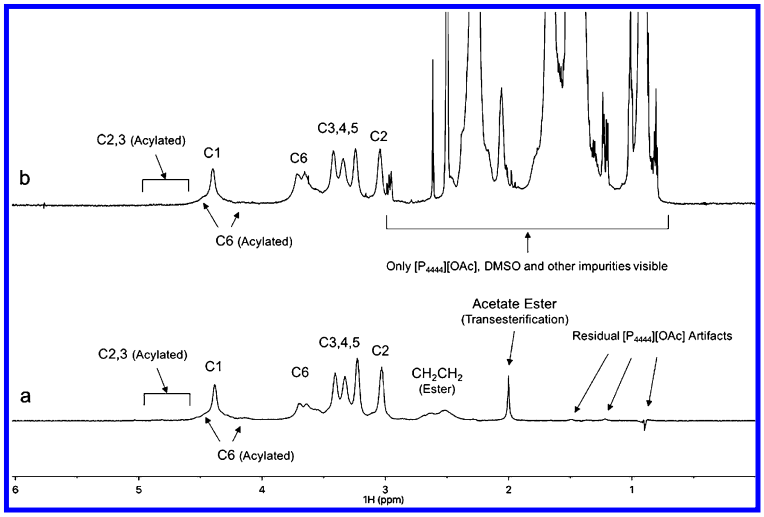

Figure 3. ^{1}H NMR analysis of the cellulose 2*H*,2*H*,3*H*,3*H*-perfluorononanoyl ester in [P_{4444}][OAc]/DMSO-d_6: diffusion-edited ^{1}H (CC-BPPSTE) spectrum, for exclusion of fast-diffusing species, such as, DMSO and ionic liquid (a), standard ^{1}H spectrum which is overwhelmed with DMSO and ionic liquid signals (b).

Herein, we also observed that the dispersibility of the cellulose 2*H*,2*H*,3*H*,3*H*-perfluorononanoyl ester in THF was enhanced. ^{13}C NMR (400 MHz): δ 27.33 ($COCH_2CH_2$), 67.58 (C6 & esterified C6), 73.65−76.93 (C2,3,5 & esterified C2,3,5), 90.87 (C4), 105−120 (CF_X), 173.28 (C═O).

Quantitative liquid-state ^{13}C NMR analysis of the 2*H*,2*H*,3*H*,3*H*-perfluorononanoyl cellulose ester was also performed in [P_{4444}][OAc]/DMSO-d_6 (Figure 2c). This allows for much better resolution and quantification of chemical species but at the loss of solid-state conformational information, that is, crystallinity information. It was observed that after dissolution of the ester (80 °C for 1 h), the mixture partially phase-separated after cooling below 50 °C. As cellulose is fully soluble in such electrolytes,[30,31] we speculated that this was due to phase separation of an enriched fluorous phase. However, for further experiments, the probe temperature was increased above the phase-separation point. For quantitative ^{13}C, it was possible to collect transients for 3 days at 90 °C using a 5 mm broad-band probe. All resonances that are visible in the ^{13}C CP MAS spectrum are also visible in the liquid-state spectrum, except the ester carbonyl and unfluorinated ester methylene carbons (α and β), which overlap with the ionic liquid resonances. For the cellulose backbone and fluorinated carbons, the resolution is much higher. Peaks which correspond to the cellulose backbone peaks are consistent with our previous assignments.[31] The signal-to-noise ratio is, however, not good enough to identify further resonances corresponding to carbons directly attached to acylated hydroxyls. On the basis of a previous NMR study of regioselective acetylated cellulose,[35] these ^{13}C resonances are not expected to deviate significantly from the unsubstituted positions; thus, they overlap with the unmodified peak clusters. The fluorinated carbons (105−120 ppm) clearly show the coupling with ^{19}F (1/2 spin quantum number), as further proof that these are in fact fluorinated carbons. Integration of this region (6 carbons) against the C2-5 peak cluster (4 carbons) allows for determination of a rough degree of substitution (DS) value of 1.15. This seems to be roughly consistent with the ^{13}C CP MAS results, which is not regarded as a quantitative technique.

The solution was also subjected to ^{1}H NMR analysis (Figure 3). Typical peaks corresponding to unmodified cellulose are clearly visible.[31] However, the ionic liquid and DMSO signals (0.8−2.8 ppm) overlap with the region where we expect to see the α and β positions on the cellulose ester substituents. To solve this problem, we optimized a CC-BPPSTE DOSY experiment such that all nonpolymeric species (fast diffusing) were edited out of the spectra. This was achieved by optimizing the encoding gradient pulse length, gradient delay, and finally the gradient increments to select for the observation of only the polymeric species in solution (slow diffusing). In the optimized experiment, only transients using the highest gradient strength were collected, that is, a single gradient, which allows for editing out of the fast diffusing species. Some artifacts persisted, corresponding to the peak positions for the ionic liquid. However, these eventually decreased in intensity, as transients were collected, relative to the polymeric cellulose resonances. Convection compensation was required, as the standard BPPSTE sequence did not fully eliminate the ionic liquid resonances after applying stronger gradients. The temperature during the whole experiment was 65 °C. Fortunately, after applying the diffusion-edited ^{1}H experiment, peaks corresponding to slow diffusing species (polymeric) were clearly visible at 2.38−2.78 ppm. The positions of these two peaks correspond nicely to the α and β positions, respectively, expected for the cellulose esters of this type.[36] In addition to the fluorinated ester resonances, there is a sharp peak at 2 ppm. This is clearly a polymeric acetate ester of cellulose, which was not introduced during the synthesis step but is an artifact of the analytical procedure, where transesterification occurs mainly during the extended quantitative ^{13}C experiment (90 °C, 3 days). This most likely occurs by the attack of the [P_{4444}][OAc] acetate anion at the fluorinated ester carbonyl, forming a mixed anhydride which then goes on to acetylate free hydroxyls on cellulose. While extensive work has not yet been carried out to confirm this unequivocally, there are practically few possible alternative explanations if followed to logical conclusions. Chemical shifts of around 2 ppm in ^{1}H NMR are characteristic of acetate esters. Peaks, between 4 and 5 ppm, underlying the main C1 resonance at 4.4 ppm are also visible, which are in the

DOI: 10.1021/acsami.7b19310
ACS Appl. Mater. Interfaces 2018, 10, 11280−11288

correct spectral region for acylated C2,3,6, according to previous assignments based on regioselectively acetylated celluloses.[35] The combined NMR for the ^{1}H and ^{13}C nuclei is very strong evidence that cellulose esters are formed, yet with a large proportion of unreacted cellulose.

To further confirm reaction, we carried out the fluoroester formation on MCC in the direct-dissolution solvent [Amim]Cl, with excess pyridine (Supporting Information).[37] A homogeneous reaction was performed and product was obtained, after precipitation of the insoluble product from the reaction media, almost immediately upon the addition of acid chloride. After performing the diffusion-edited ^{1}H experiment on the product, the same broad peak centered at 2.5 ppm for the polymeric ester CH_2 was present (Figure S11). In the homogeneous reaction, the acetate signal at 2 ppm was of rather low intensity after dissolution in the electrolyte NMR solution. The acetate signal was also observed to increase with extended heating. This gives strong support to the transesterification mechanism for the introduction of acetate to the polymer, as it is difficult to imagine how it might be introduced via any other mechanism.

The crystallinity of fluorinated cellulose esters was investigated by XRD and solid-state ^{13}C CP MAS NMR. XRD patterns obtained from native CNCs, fluorinated cellulose esters, and also nanostructured fluorinated cellulose esters samples are shown in Figures 4 and S4. The reduced intensity

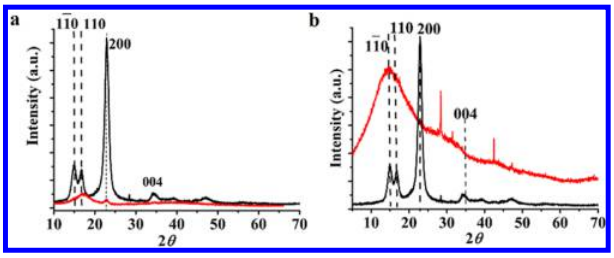

Figure 4. XRD of native CNCs (black curves) (a,b), cellulose 2*H*,2*H*,3*H*,3*H*-perfluorononanoyl ester before the nanoprecipitation dropping technique (red curve) (a) and NPs of the cellulose 2*H*,2*H*,3*H*,3*H*-perfluorononanoyl ester after the nanoprecipitation dropping technique (red curves) (b).

of the peak at the 200-plane demonstrates the reduction of crystalline-ordered scattering units. However, this may not result from a significant destruction of the crystalline structure but rather a reduction in the scattering intensity attributed to the crystalline regions because of the reduced cellulose content and to the consumption of the incident and scattering intensity because of the high fluorine content. An increased intensity is found in the amorphous region of cellulose esters at around 2θ = 18°, which could be attributed to the less ordered region of cellulose chains[38] but is also equally attributable to other amorphous materials. The XRD peaks of nanostructure cellulose esters acquire broader peaks at lower angles. These peaks may appear from a smaller size of cellulose crystallites. However, it has to be considered that an amorphous region of disordered cellulose esters or an amorphous ester can emerge at 2θ angles around 18°−20°.[39] Nevertheless, the diffractograms for the cellulose 2*H*,2*H*,3*H*,3*H*-perfluorononanoyl ester immediately suggest an increase in amorphous structure in the absence and strong reduction of all peaks corresponding to planes $1\bar{1}0$, 110, and 200. However, there is stronger evidence from the ^{13}C CP MAS deconvolution. In particular, C4 peaks of solid-state ^{13}C NMR on cellulose are particularly appropriate to determine the relative crystalline allomorph and amorphous contents in solid cellulose. When applying deconvolution of the C4 region, according to Wickholm et al.[40] (Supporting Information), the reference unmodified CNC gives a crystallinity index (CI) of 78.9%. When applying the deconvolution to the cellulose 2*H*,2*H*,3*H*,3*H*-perfluorononanoyl ester, a CI of 66.5% is obtained, for the cellulosic portion of the sample, i.e., not including the mass associated with the fluorinated ester functionalities. This is not such a significant reduction in crystallinity, for the cellulosic portion and most likely close to the error margin, considering that there are additional broad resonances unaccounted for. Considering a DS of 1.15, the crystallinity of the material reduces to 18.2%. In other words, there is nanocellulose remaining in the sample. The reaction is clearly heterogeneous but yielding, most likely soluble, amorphous cellulose ester coprecipitated with the nanocellulose. On the basis of the X-ray diffractograms, after the nanoprecipitation procedure, the peaks attributable to cellulose crystallinity are completely missing. The sharp peak that is located at 2θ = 28° in Figure 4b is related to the Si substrate.[41] This indicates that insoluble cellulose nanocrystallites are filtered out during the filter-paper filtration step, and the colloidal dispersion/solution of the modified cellulose passes through. This also indicates that the actual DS of the soluble (during the modification reaction) cellulose ester is actually higher than 1.15. As the reaction with CNCs is a heterogeneous reaction, not requiring the use of expensive ionic liquids, the lower molecular weight and high surface area CNCs offer an increase in reactivity. However, the method might also be applicable to MCC. Clearly, further work is required to characterize the reaction in detail, for further optimization.

3.2. Nanoprecipitation and Paper Hydrophobization.

In the literature, two different techniques are applied for manufacturing polymeric NPs, namely, dialysis and dropping techniques.[42] Nanoprecipitation is interesting for preparing colloids for stabilizing pigments[43] and also industrially important components in paints, lacquers, and other coatings.[44] The strong hydrogen-bonding network and the hydrophobic interactions of CNCs prevent dissolution into most common organic solvents. However, the solubility of cellulose and dispersibility of CNCs can clearly be improved by surface functionalization. Increasing solubility of cellulose esters and providing a stable dispersion of nanostructured cellulose esters are crucial factors to obtain more uniform coatings on different surfaces. Solubility of fluorinated cellulose esters was tested in different nonpolar solvents. Previously, this has been dependent on the DS and the chain length of the acyl chlorides.[45] Both cellulose esters reported here are mostly insoluble in nonpolar solvents (such as hexane, pentane, benzene, and toluene), while THF was a pretty good solvent for dispersion, compared to other solvents. Therefore, THF was chosen to allow for initial dispersion of the cellulose ester into deionized water using the nanoprecipitation dropping technique.

The size and shape of nanostructured fluorinated cellulose esters were analyzed by scanning electron microscopy (SEM) and dynamic light scattering (DLS). SEM shows that the NPs of the cellulose 2*H*,2*H*,3*H*,3*H*-perfluorononanoyl ester have a spherical shape with an average diameter of 83 nm by ImageJ software (n = 50) (Figure 5), while nanostructured fluorinated cellulose esters resulting from the nanoprecipitation dropping technique had an average diameter of 184 nm with a polydispersity index of 0.309 (Figure 6).

DOI: 10.1021/acsami.7b19310
ACS Appl. Mater. Interfaces 2018, 10, 11280−11288

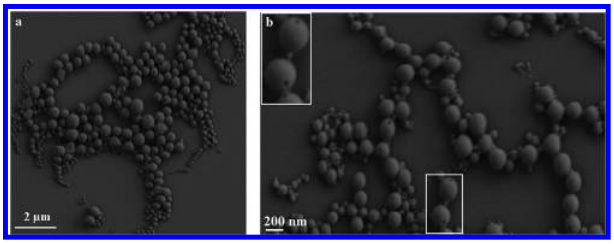

Figure 5. SEM images of NPs of the cellulose 2*H*,2*H*,3*H*,3*H*-perfluorononanoyl ester with a scale bar of 2 μm (a) and 200 nm (b).

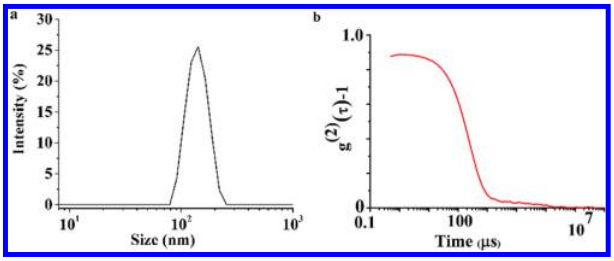

Figure 6. Size distribution of cellulose 2*H*,2*H*,3*H*,3*H*-perfluorononanoyl ester NPs based on DLS measurement (a) and corresponding autocorrelation curve (b).

The difference between average diameters obtained from SEM and DLS may be related to the sample preparation for the different techniques. In the DLS measurement, the fluorinated cellulose ester NPs may be slightly swollen in deionized water. Thus, they show larger hydrodynamic diameters. On the contrary, samples were dried for SEM measurement.

As shown in Figure 5, this nanoprecipitation technique also led to the formation of nanospheres with holes in their surfaces (less than 25 nm in diameter). In fact, evaporation of THF led to form a hole in the surface of each NP, similarly as Xia et al. had observed for polystyrene spheres.[46] These cellulose NPs with holes may open new pathways to selective encapsulation and delivery.

Because cellulose esters interact poorly with water, the formation of NPs is based on the aggregation of cellulose ester chains during diffusion of drops of cellulose dispersion into deionized water.[29] In this fast process, there is a large contact area between the drops of fluorinated cellulose ester dispersion and water which promotes the diffusion of THF and therefore the aggregation of cellulose ester chains.[29] After removal of THF, cellulose esters start shrinking, and eventually, nanospherical cellulose esters are formed.

Spin-coating was applied in the present study for hydrophobization and superhydrophobization of paper. A4 paper was used for the experiments. The contact angles of paper after coating are bigger than 150°, while the uncoated paper is very hydrophilic and water droplets penetrate inside of the paper easily after only a few seconds. As well, more homogeneous hydrophobized paper was obtained by utilization of more dilute nanostructured fluorinated cellulose ester dispersion.

As was mentioned previously, the dispersibility of modified cellulose esters in organic solvents such as THF was increased when the molar ratio of fluorinated acid chloride to CNCs was enhanced. Recently, the superhydrophobic surface on the paper[22] and glass[26] with the nanostructured cellulose stearoyl ester[29] has been constructed. Geissler et al. indicated that the initial concentration of the cellulose ester dispersion and the fabrication method affect the size of the obtained cellulose ester NPs.[29] In fact, the concentration of fluorinated cellulose ester dispersion should be at least 5 mg/mL to make the superhydrophobic paper. The contact angle hysteresis was 40 ± 2° (Figure 7).

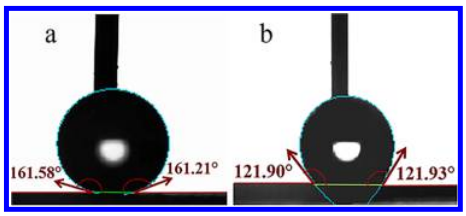

Figure 7. Advancing (a) and receding (b) contact angles of the surface with cellulose the 2*H*,2*H*,3*H*,3*H*-perfluorononanoyl ester.

Additionally, the effect of the attached fluoroalkyl group on the cellulose surface and also the nanoprecipitation technique was investigated by SEM. Obviously, fluoro functional groups help to enhance hydrophobicity of final nanostructured fluorinated cellulose esters. However, the requirement for a nanoscale starting material, such as CNCs, is not clear. Lower cost substrates may be possible, particularly if an economical heterogeneous reaction is to be applied. Clearly, the superhydrophobicity can be improved using high DS of cellulose esters. The DS of cellulose esters is known to be of course influenced by the ratio of acyl chloride-to-cellulose hydroxyl groups, degrees of polymerization, solvent temperature, and volume. However, for heterogeneous reactions, the highest achievable DS may also be dictated by the solubility of the modified polymer in the reaction media. In this case, formation phases partly controlled by fluorous interactions (in pyridine/toluene or THF) may be critical in controlling both the DS and formation of nanospheres.

Figure 8a shows the surface-sensitive XPS data of the coated paper surface. According to XPS data, the surface region of the fluorinated NPs consisted of carbon, oxygen, and fluorine; see the survey spectra in Figure 8a. The chemical bonding of the fluorine groups, which are considered to be the underlying reasons for the superhydrophobicity of the paper, were characterized in detail from the high-resolution carbon C 1s. The presence of two chemically different cellulosic carbons (C−C/C−O/O−C−O) in the characteristic ratio, as well as carbons with either two or three fluorine atoms (CF_2 and CF_3), and the carbon with three oxygen neighbors (C≡O) for the esterification, were all well-resolved in the deconvoluted C 1s spectrum of the modified cellulose sample (see insert in Figure 8a). Carbon atoms with one and two bonds to oxygen neighbors show the cellulosic fingerprint, while carbon atoms with two or three bonds to fluorine atoms and the carbon with three bonds to oxygen are due to esterification. Rough surface morphology of the coated paper was also observed by SEM (Figure 8b,c). The SEM images also showed the presence of the nano-/microstructured fluorinated cellulose ester which was preserved after the spin-coating process.

3.3. Environmental and (Eco)toxicological Considerations. Although per- and polyfluorinated substances and their respective polymers, because of their superior performance and stability,[47−50] have been and still are almost ubiquitously used in a wide variety of applications,[11,48,51,52] numerous concerns pertaining to their environmental and toxicological effects have recently arisen.[53,54] Long-chain compounds (with seven or

DOI: 10.1021/acsami.7b19310
ACS Appl. Mater. Interfaces 2018, 10, 11280−11288

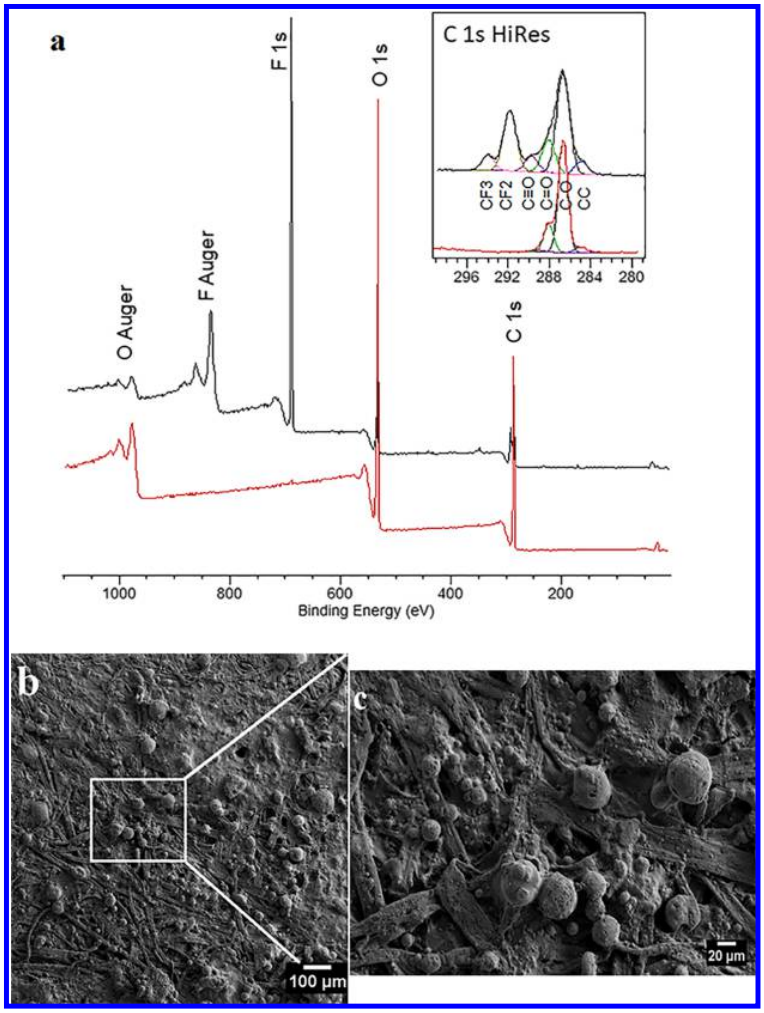

Figure 8. X-ray photoelectron spectroscopy (XPS) data shows the chemical surface composition within the topmost 5 nm (a). Data recorded from the cellulose ester are depicted in black, whereas data from the reference sample, Whatman filter paper, are shown in red. Elemental composition is shown in the wide energy region spectra, while more detailed data on carbon compounds are depicted in the curve-fitted high-resolution spectra of the C 1s region. SEM images of superhydrophobic paper at different magnifications with a scale bar of (b) 100 μm and (c) 20 μm.

more perfluorinated carbons), such as perfluorooctanoic acid or perfluorooctanesulfonic acid and their respective salts, have already been taken off the market or are currently undergoing phase-out procedures.[48,55] In general, it is presumed that the longer the perfluorinated chain, the more problematic the substance is going to be in terms of bioaccumulation and toxicity. Consequently, shorter-chain (six carbons or less) perfluorinated compounds are, for now, allowed to remain in use and currently attract unprecedented scientific interest.

The aforementioned points make it all the more noteworthy that we found the 2*H*,2*H*,3*H*,3*H*-perfluorononanoyl-functionalized cellulose to exhibit higher hydrophobicity (demonstrated by its superior dispersibility) than its 2*H*,2*H*,3*H*,3*H*-perfluoroundecanoyl-derived counterpart. This of course may also be due to the ability of the heterogeneous procedure to derivatize the CNCs to a higher DS using the 2*H*,2*H*,3*H*,3*H*-perfluorononanoyl reagent, presumably as a function of the reagent solubility in the reaction media. While CNCs modified with 2*H*,2*H*,3*H*,3*H*-perfluoroheptanoyl groups would arguably be even more environmentally benign, it is as yet unknown if they will form NPs through this nanodispersion method. This may depend on the reachable DS under the reaction conditions. However, it may also depend on factors, such as propensity to form crystalline phases due to side-chain interactions, which diminishes as the perfluorinated chain length decreases.[56] More approximately, when the fluorous content decreases, it gives way to preferential hydrophilic interactions between the water droplet and the hydrophilic cellulosic backbone.

4. CONCLUSIONS

The main findings of this work can be divided into two parts. First, we gained access to superhydrophobic fluorinated cellulose esters by the esterification of CNCs under heterogeneous conditions, that is, not all of the CNCs were converted to a dispersible product but some unreacted cellulose remained. This mitigates the use of expensive direct-dissolution solvents, but more work is required to understand and optimize this chemistry. The materials were characterized by both liquid-state NMR and several solid-state techniques. Second, spin-coating was applied to translate the superhydrophobic property of the modified cellulose to the surfaces of several substrates. The modification efficiency was probed by spectrometric

DOI: 10.1021/acsami.7b19310
ACS Appl. Mater. Interfaces 2018, 10, 11280−11288

analysis and the examination of dispersion properties. We demonstrated that the fluorinated cellulose ester provides a more transparent dispersion in THF. Solid-state ^{13}C NMR and XRD analyses showed that cellulose crystallinity was retained during the preparation step but that this is essentially removed during the filtration and nanoprecipitation techniques, yielding nanospheres. In other words, the reaction is heterogeneous but yields an amorphous nanodispersible fluorinated cellulose ester. Paper with superhydrophobic surface properties may find applications in packaging materials, textiles, outdoor clothing, and microfluidic devices. In the future, it would be highly interesting to develop a way, such as optimization of DS, to achieve a more stable and uniform superhydrophobic surface on various substrates such as glass or textiles.

■ ASSOCIATED CONTENT

Supporting Information

The Supporting Information is available free of charge on the ACS Publications website at DOI: 10.1021/acsami.7b19310.

Synthesis and characterization of 2*H*,2*H*,3*H*,3*H*-perfluorononanoyl chloride and the cellulose 2*H*,2*H*,3*H*,3*H*-perfluoroundecanoyl ester (PDF)

■ AUTHOR INFORMATION

Corresponding Author

*E-mail: robin.ras@aalto.fi.

ORCID

Alistair W. T. King: 0000-0003-3142-9259

Mauri A. Kostiainen: 0000-0002-8282-2379

Robin H. A. Ras: 0000-0002-2076-242X

Author Contributions

The manuscript was written through contributions of all authors. All authors have given approval to the final version of the manuscript.

Notes

The authors declare no competing financial interest.

■ ACKNOWLEDGMENTS

This work was supported by the European Research Council ERC-2016-CoG (725513-SuperRepel) and Academy of Finland (Centres of Excellence Programme (2014−2019)). This work made use of the Aalto University Nanomicroscopy Centre premises. The authors acknowledge Taneli Tiittanen for his help in the XRD measurements. The authors would also like to acknowledge the Academy of Finland for funding under the project 'WTF-Click-Nano' (311255).

■ ABBREVIATIONS

CNCs, cellulose nanocrystals; MCC, microcrystalline cellulose; CA, contact angle; DLS, dynamic light scattering; SEM, scanning electron microscopy; XRD, X-ray diffraction; NP, nanoparticle; CP MAS, cross-polarizing magic-angle spinning; CC-BPPSTE, convection compensated bipolar pulse pair stimulated echo; DOSY, diffusion-ordered spectroscopy; DS, degree of substitution; CI, crystallinity index; NMR, nuclear magnetic resonance (spectroscopy)

■ REFERENCES

(1) Lafuma, A.; Quéré, D. Superhydrophobic States. *Nat. Mater.* **2003**, *2*, 457−460.

(2) Guo, Z.; Liu, W.; Su, B.-L. Superhydrophobic Surfaces: From Natural to Biomimetic to Functional. *J. Colloid Interface Sci.* **2011**, *353*, 335−355.

(3) Ma, M.; Hill, R. M. Superhydrophobic Surfaces. *Curr. Opin. Colloid Interface Sci.* **2006**, *11*, 193−202.

(4) Verho, T.; Bower, C.; Andrew, P.; Franssila, S.; Ikkala, O.; Ras, R. H. A. Mechanically Durable Superhydrophobic Surfaces. *Adv. Mater.* **2011**, *23*, 673−678.

(5) Tian, Y.; Su, B.; Jiang, L. Interfacial Material System Exhibiting Superwettability. *Adv. Mater.* **2014**, *26*, 6872−6897.

(6) Yan, Y. Y.; Gao, N.; Barthlott, W. Mimicking Natural Superhydrophobic Surfaces and Grasping The Wetting Process: A Review On Recent Progress In Preparing Superhydrophobic Surfaces. *Adv. Colloid Interface Sci.* **2011**, *169*, 80−105.

(7) Roach, P.; Shirtcliffe, N. J.; Newton, M. I. Progess In Superhydrophobic Surface Development. *Soft Matter* **2008**, *4*, 224−240.

(8) Li, X.-M.; Reinhoudt, D.; Crego-Calama, M. What Do We Need For a Superhydrophobic Surface? A Review On The Recent Progress In The Preparation Of Superhydrophobic Surfaces. *Chem. Soc. Rev.* **2007**, *36*, 1350−1368.

(9) Crick, C. R.; Parkin, I. P. Preparation and Characterisation of Super-Hydrophobic Surfaces. *Chem.—Eur. J.* **2010**, *16*, 3568−3588.

(10) Ras, R. H. A.; Tian, X.; Bayer, I. S. Superhydrophobic and Superoleophobic Nanostructured Cellulose and Cellulose Composites. In Handbook of Nanocellulose and Cellulose Nanocomposites Superhydrophobic and Superoleophobic Nanostructured Cellulose and Cellulose Composites. *Handbook of Nanocellulose and Cellulose Nanocomposites*; Wiley-VCH Verlag GmbH & Co. KGaA: Weinheim, Germany, 2017; pp 731−760.

(11) Song, J.; Rojas, O. J. Approaching Super-Hydrophobicity from Cellulosic Materials: A Review. *Nord. Pulp Pap. Res. J.* **2013**, *28*, 216−238.

(12) Wen, Q.; Guo, F.; Yang, F.; Guo, Z. Green Fabrication of Coloured Superhydrophobic Paper from Native Cotton Cellulose. *J. Colloid Interface Sci.* **2017**, *497*, 284−289.

(13) Baidya, A.; Ganayee, M. A.; Ravindran, S. J.; Tam, K. C.; Das, S. K.; Ras, R. H. A.; Pradeep, T. Organic Solvent-Free Fabrication of Durable and Multifunctional Superhydrophobic Paper from Waterborne Fluorinated Cellulose Nanofiber Building Blocks. *ACS Nano* **2017**, *11*, 11091−11099.

(14) Balu, B.; Kim, J. S.; Breedveld, V.; Hess, D. W. Tunability of the Adhesion of Water Drops on a Superhydrophobic Paper Surface via Selective Plasma Etching. *J. Adhes. Sci. Technol.* **2009**, *23*, 361−380.

(15) Hu, Z.; Zen, X.; Gong, J.; Deng, Y. Water Resistance Improvement of Paper by Superhydrophobic Modification with Microsized $CaCO_3$ and Fatty Acid Coating. *Colloids Surf., A* **2009**, *351*, 65−70.

(16) Werner, O.; Quan, C.; Turner, C.; Pettersson, B.; Wågberg, L. Properties of Superhydrophobic Paper Treated with Rapid Expansion of Supercritical CO2 Containing a Crystallizing Wax. *Cellulose* **2010**, *17*, 187−198.

(17) Quan, C.; Werner, O.; Wågberg, L.; Turner, C. Generation of Superhydrophobic Paper Surfaces by a Rapidly Expanding Supercritical Carbon Dioxide−alkyl Ketene Dimer Solution. *J. Supercrit. Fluids* **2009**, *49*, 117−124.

(18) Yang, H.; Deng, Y. Preparation and Physical Properties of Superhydrophobic Papers. *J. Colloid Interface Sci.* **2008**, *325*, 588−593.

(19) Arbatan, T.; Zhang, L.; Fang, X.-Y.; Shen, W. Cellulose Nanofibers as Binder for Fabrication of Superhydrophobic Paper. *Chem. Eng. J.* **2012**, *210*, 74−79.

(20) Carlmark, A.; Malmström, E. E. ATRP Grafting from Cellulose Fibers to Create Block-Copolymer Grafts. *Biomacromolecules* **2003**, *4*, 1740−1745.

(21) Carlmark, A.; Malmström, E. Atom Transfer Radical Polymerization from Cellulose Fibers at Ambient Temperature. *J. Am. Chem. Soc.* **2002**, *124*, 900−901.

(22) Geissler, A.; Loyal, F.; Biesalski, M.; Zhang, K. Thermo-Responsive Superhydrophobic Paper Using Nanostructured Cellulose Stearoyl Ester. *Cellulose* **2014**, *21*, 357−366.
(23) Klemm, D.; Heublein, B.; Fink, H.-P.; Bohn, A. Cellulose: Fascinating Biopolymer and Sustainable Raw Material. *Angew. Chem., Int. Ed. Engl.* **2005**, *44*, 3358−3393.
(24) Nyström, D.; Lindqvist, J.; Östmark, E.; Hult, A.; Malmström, E. Superhydrophobic Bio-Fibre Surfaces via Tailored Grafting Architecture. *Chem. Commun.* **2006**, *34*, 3594−3596.
(25) Liebert, T.; Hänsch, C.; Heinze, T. Click Chemistry with Polysaccharides. *Macromol. Rapid Commun.* **2006**, *27*, 208−213.
(26) Geissler, A.; Chen, L.; Zhang, K.; Bonaccurso, E.; Biesalski, M. Superhydrophobic Surfaces Fabricated from Nano- and Micro-structured Cellulose Stearoyl Esters. *Chem. Commun.* **2013**, *49*, 4962−4964.
(27) Majoinen, J.; Walther, A.; McKee, J. R.; Kontturi, E.; Aseyev, V.; Malho, J. M.; Ruokolainen, J.; Ikkala, O. Polyelectrolyte Brushes Grafted from Cellulose Nanocrystals Using Cu-Mediated Surface-Initiated Controlled Radical Polymerization. *Biomacromolecules* **2011**, *12*, 2997−3006.
(28) Edgar, C. D.; Gray, D. G. Smooth Model Cellulose I Surfaces from Nanocrystal Suspensions. *Cellulose* **2003**, *10*, 299−306.
(29) Geissler, A.; Biesalski, M.; Heinze, T.; Zhang, K. Formation of Nanostructured Cellulose Stearoyl Esters via Nanoprecipitation. *J. Mater. Chem. A* **2014**, *2*, 1107−1116.
(30) Holding, A. J.; Heikkilä, M.; Kilpeläinen, I.; King, A. W. T. Amphiphilic and Phase-Separable Ionic Liquids for Biomass Processing. *ChemSusChem* **2014**, *7*, 1422−1434.
(31) Holding, A. J.; Mäkelä, V.; Tolonen, L.; Sixta, H.; Kilpeläinen, I.; King, A. W. T. Solution-State One- and Two-Dimensional NMR Spectroscopy of High-Molecular-Weight Cellulose. *ChemSusChem* **2016**, *9*, 880−892.
(32) Wu, D. H.; Chen, A. D.; Johnson, C. S. An Improved Diffusion-Ordered Spectroscopy Experiment Incorporating Bipolar-Gradient Pulses. *J. Magn. Reson., Ser. A* **1995**, *115*, 260−264.
(33) Jerschow, A.; Müller, N. Suppression of Convection Artifacts in Stimulated-Echo Diffusion Experiments. Double-Stimulated-Echo Experiments. *J. Magn. Reson.* **1997**, *125*, 372−375.
(34) Korhonen, J. T.; Huhtamäki, T.; Ikkala, O.; Ras, R. H. A. Reliable Measurement of the Receding Contact Angle. *Langmuir* **2013**, *29*, 3858−3863.
(35) Karakawa, M.; Mikawa, Y.; Kamitakahara, H.; Nakatsubo, F. Preparations of Regioselectively Methylated Cellulose Acetates and Their ^{1}H and ^{13}C NMR Spectroscopic Analyses. *J. Polym. Sci., Part A: Polym. Chem.* **2002**, *40*, 4167−4179.
(36) Fisch, D.; Gruhl, C.; Kalkowski, E.; Sick, B.; Ovaska, S. J. Towards Automation of Knowledge Understanding: An Approach for Probabilistic Generative Classifiers. *Inf. Sci.* **2016**, *370*−*371*, 476−496.
(37) Kyllönen, L.; Parviainen, A.; Deb, S.; Lawoko, M.; Gorlov, M.; Kilpeläinen, I.; King, A. W. T. On the Solubility of Wood in Non-Derivatising Ionic Liquids. *Green Chem.* **2013**, *15*, 2374−2378.
(38) Segal, L.; Creely, J. J.; Martin, A. E.; Conrad, C. M. An Empirical Method for Estimating the Degree of Crystallinity of Native Cellulose Using the X-Ray Diffractometer. *Text. Res. J.* **1959**, *29*, 786−794.
(39) Jandura, P.; Kokta, B. V.; Riedl, B. Fibrous Long-Chain Organic Acid Cellulose Esters and Their Characterization by Diffuse Reflectance FTIR Spectroscopy, Solid-State CP/MAS ^{13} C-NMR, and X-Ray Diffraction. *J. Appl. Polym. Sci.* **2000**, *78*, 1354−1365.
(40) Wickholm, K.; Larsson, P. T.; Iversen, T. Assignment of Non-Crystalline Forms in Cellulose I by CP/MAS ^{13}C NMR Spectroscopy. *Carbohydr. Res.* **1998**, *312*, 123−129.
(41) Morris, M. C.; McMurdie, H. F.; Evans, E. H.; Paretzkin, B.; de Groot, J. H.; Hubbard, C. R.; Carmel, S. j. Standard X-Ray Diffraction Powder Patterns. In Nat. Bur. Stand. (U.S.) Monoger.; 1976; p 114.
(42) Hornig, S.; Heinze, T.; Becer, C. R.; Schubert, U. S. Synthetic Polymeric Nanoparticles by Nanoprecipitation. *J. Mater. Chem.* **2009**, *19*, 3838−3840.
(43) Radley, J. A. U.S. Patent 2,506,892 A, 1950.
(44) Schubert, S.; Delaney, J. T., Jr.; Schubert, U. S. Nanoprecipitation and Nanoformulation of Polymers: From History to Powerful Possibilities beyond Poly(lactic Acid). *Soft Matter* **2011**, *7*, 1581−1588.
(45) Nagel, M. C. V.; Heinze, T. Study about the Efficiency of Esterification of Cellulose under Homogenous Condition: Dependence on the Chain Length and Solvent. *Lenzinger Ber.* **2012**, *90*, 85−92.
(46) Im, H. S.; Jeong, U.; Xia, Y. Polymer Hollow Particles with Controllable Holes in Their Surfaces. *Nat. Mater.* **2005**, *4*, 671−675.
(47) Hummel, M.; Markiewicz, M.; Stolte, S.; Noisternig, M.; Braun, D. E.; Gelbrich, T.; Griesser, U. J.; Partl, G.; Naier, B.; Wurst, K.; Krüger, B.; Kopacka, H.; Laus, G.; Huppertz, H.; Schottenberger, H. Phase-out-Compliant Fluorosurfactants: Unique Methimazolium Derivatives Including Room Temperature Ionic Liquids. *Green Chem.* **2017**, *19*, 3225−3237.
(48) Lindstrom, A. B.; Strynar, M. J.; Libelo, E. L. Polyfluorinated Compounds: Past, Present, and Future. *Environ. Sci. Technol.* **2011**, *45*, 7954−7961.
(49) Krafft, M. P.; Riess, J. G. Selected Physicochemical Aspects of Poly- and Perfluoroalkylated Substances Relevant to Performance, Environment and Sustainability-Part One. *Chemosphere* **2015**, *129*, 4−19.
(50) Czajka, A.; Hazell, G.; Eastoe, J. Surfactants at the Design Limit. *Langmuir* **2015**, *31*, 8205−8217.
(51) Radaelli, G.; Heredia-Guerrero, J. A.; Masood, M. T.; Ceseracciu, L.; Davis, A.; Carzino, R.; Prato, M.; Bayer, I. S.; Athanassiou, A. Highly Effective Antiadhesive Coatings from pH-Modified Water-Dispersed Perfluorinated Acrylic Copolymers: The Case of Vulcanizing Rubber. *Adv. Mater. Interfaces* **2016**, *3*, 1600069.
(52) Hagenaars, A.; Meyer, I. J.; Herzke, D.; Pardo, B. G.; Martinez, P.; Pabon, M.; De Coen, W.; Knapen, D. The Search for Alternative Aqueous Film Forming Foams (AFFF) with a Low Environmental Impact: Physiological and Transcriptomic Effects of Two Forafac Fluorosurfactants in Turbot. *Aquat. Toxicol.* **2011**, *104*, 168−176.
(53) Kannan, K.; Corsolini, S.; Falandysz, J.; Fillmann, G.; Kumar, K. S.; Loganathan, B. G.; Mohd, M. A.; Olivero, J.; Van Wouwe, N.; Yang, J. H.; Aldous, K. M. Perfluorooctanesulfonate and Related Fluorochemicals in Human Blood from Several Countries. *Environ. Sci. Technol.* **2004**, *38*, 4489−4495.
(54) Olsen, G. W.; Ellefson, M. E.; Mair, D. C.; Church, T. R.; Goldberg, C. L.; Herron, R. M.; Medhdizadehkashi, Z.; Nobiletti, J. B.; Rios, J. A.; Reagen, W. K.; Zobel, L. R. Analysis of a Homologous Series of Perfluorocarboxylates from American Red Cross Adult Blood Donors, 2000-2001 and 2006. *Environ. Sci. Technol.* **2011**, *45*, 8022−8029.
(55) ECHA. *Annex XV Restriction Report - Proposal for a Restriction*, version 1.0, 17; 2014.
(56) Honda, K.; Morita, M.; Otsuka, H.; Takahara, A. Molecular Aggregation Structure and Surface Properties of Poly(fluoroalkyl Acrylate) Thin Films. *Macromolecules* **2005**, *38*, 5699−5705.

DOI: 10.1021/acsami.7b19310
ACS Appl. Mater. Interfaces 2018, 10, 11280−11288